



Cite this: *Phys. Chem. Chem. Phys.*,  
2018, 20, 16393

## Towards a full quantitative description of single-molecule reaction kinetics in biological cells†

Denis S. Grebenkov, \*<sup>a</sup> Ralf Metzler <sup>b</sup> and Gleb Oshanin <sup>c</sup>

The first-passage time (FPT), *i.e.*, the moment when a stochastic process reaches a given threshold value for the first time, is a fundamental mathematical concept with immediate applications. In particular, it quantifies the statistics of instances when biomolecules in a biological cell reach their specific binding sites and trigger cellular regulation. Typically, the first-passage properties are given in terms of mean first-passage times. However, modern experiments now monitor single-molecular binding-processes in living cells and thus provide access to the full statistics of the underlying first-passage events, in particular, inherent cell-to-cell fluctuations. We here present a robust explicit approach for obtaining the distribution of FPTs to a small partially reactive target in cylindrical-annulus domains, which represent typical bacterial and neuronal cell shapes. We investigate various asymptotic behaviours of this FPT distribution and show that it is typically very broad in many biological situations, thus, the mean FPT can differ from the most probable FPT by orders of magnitude. The most probable FPT is shown to strongly depend only on the starting position within the geometry and to be almost independent of the target size and reactivity. These findings demonstrate the dramatic relevance of knowing the full distribution of FPTs and thus open new perspectives for a more reliable description of many intracellular processes initiated by the arrival of one or few biomolecules to a small, spatially localised region inside the cell.

Received 30th March 2018,  
Accepted 21st May 2018

DOI: 10.1039/c8cp02043d

rsc.li/pccp

### 1. Introduction

Many intracellular processes of signalling, regulation, infection, immune reactions, metabolism, or transmitter release in neurons are triggered by the arrival of one or few biomolecules to a small spatially localised region.<sup>1,2</sup> Such processes determine the cellular function and are controlled by the statistics of the first-passage time (FPT) to a reaction event (also called the reaction time), *i.e.*, the instant in time when the respective molecules hit their target site for the first time and initiate biochemical responses.<sup>3–8</sup> With modern techniques such as super-resolution microscopy, it is possible to monitor individual, single-molecular biochemical regulation and production processes in living cells, revealing, for instance, pronounced fluctuations of production events of individual messenger RNA or proteins within a single cell as well as striking differences of production patterns between genetically identical cells.<sup>9–11</sup>

Most available analytical results to quantify the first-passage dynamics were obtained for the mean first-passage time (MFPT),<sup>12–30</sup> corresponding to the inverse of the mean rate constant conventionally used in biochemistry. For a bounded domain the MFPT is typically proportional to the domain volume, and it diverges as the target region shrinks. In particular, for the so-called narrow escape problem, which pertains to a variety of situations when a diffusive particle has to leave a bounded domain through a very small window on its boundary,<sup>30,31</sup> the MFPT determines the characteristic decay time of the exponential long-time tail of the distribution of the FPT, likewise, in the case of a small target inside bounded circular domains.<sup>32,33</sup> This signifies that the MFPT is dominated by rather rare, anomalously long searching trajectories, and thus can be non-representative of the actual behaviour, or, at least be not the only important characteristic time-scale. Indeed, if a particle with diffusion coefficient  $D$  is released within a short distance  $\delta$  to the target, the relevant time scale would be  $\delta^2/D$ , whereas the MFPT would be of the order of  $L^2/D$ , where  $L$  is the size of the domain. As a consequence, in this case the kinetics of the aforementioned biological processes will most likely be determined by the most probable FPT, which can be orders of magnitude smaller than the MFPT, a scenario recently called the few-encounter limit.<sup>32</sup> Moreover, it was shown that two FPT events in the same system may be dramatically disparate.<sup>34–36</sup> In these common and biologically relevant situations, the whole FPT distribution is needed to adequately quantify the molecular

<sup>a</sup> Laboratoire de Physique de la Matière Condensée (UMR 7643), CNRS – Ecole Polytechnique, University Paris-Saclay, 91128 Palaiseau, France.  
E-mail: denis.grebenkov@polytechnique.edu

<sup>b</sup> Institute of Physics & Astronomy, University of Potsdam, 14476 Potsdam-Golm, Germany. E-mail: rmetzler@uni-potsdam.de

<sup>c</sup> Sorbonne Université, CNRS, Laboratoire de Physique Théorique de la Matière Condensée (UMR CNRS 7600), 4 Place Jussieu, F-75005, Paris, France.  
E-mail: oshanin@lptmc.jussieu.fr

† Electronic supplementary information (ESI) available. See DOI: 10.1039/c8cp02043d

process and to meaningfully extract the kinetic parameters from measurements.

However, the exact FPT distribution is known only for few elementary cases such as the FPT to a perfectly reactive target placed at the centre of a spherical region or to its boundary, starting from a fixed location.<sup>3</sup> At the same time, already finding the distribution of FPTs to a small target region on the otherwise reflecting boundary of a sphere remains an open problem. To our knowledge, the only nontrivial case, for which an exact FPT distribution was recently derived, is that of an arc-shaped target on the boundary of a disk.<sup>39</sup> To study the FPT in more complicated realistic geometries, some approximate techniques have been developed, such as the uniform approximation<sup>40</sup> and the asymptotically exact Newton-series approach.<sup>32</sup> Otherwise, one resorts to the numerical analysis of the full FPT distribution.<sup>41</sup> We emphasise that an impact of a finite reactivity on the form of the FPT distribution remains a completely open question.

We here report the approximate, but explicit and very accurate expression for the distribution of the FPT to a partially reactive annular target on a cylinder, surrounded by a larger impermeable cylinder and capped by two parallel planes (Fig. 1), which is the relevant geometry to describe the first passage of molecules to the nucleoid region of bacteria cells or to a central filament trail in the axon of a neuronal cell. Another example of such a geometry is provided by a usual experimental setup for the analysis of a diffusive search by a transcription factor protein for a specific binding site on a single strand of elongated DNA (inner cylinder), with the outer cylinder being the wall of the container. We also note that from a mathematical point of view, the method underlying the derivation of this FPT distribution can be formally generalised to arbitrary bounded domains with a small target region, and thus become applicable to the narrow escape problem in the presence of a barrier at the escape window.

Our solution relies on the self-consistent approximation (SCA) technique originally devised by Shoup, Lipari, and Szabo<sup>37</sup>

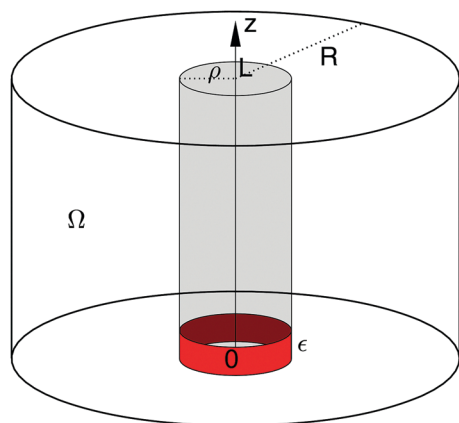


**Fig. 1** Schematic presentation of the cylindrical-annulus domain  $\Omega$  between two concentric cylinders of radii  $\rho$  and  $R$  and capped by planes at  $z = 0$  and  $z = L$ . The target region is the red annulus of radius  $\rho$  and height  $\epsilon$ .

for the analysis of reaction rates between particles with inhomogeneous reactivity, and recently applied to the MFPT in spherical<sup>28</sup> and cylindrical geometries.<sup>38</sup> Within this approximation, the exact mixed boundary condition is replaced by an effective one, reducing the problem to finding self-consistent solutions. We adapt this approximation to the modified Helmholtz equation governing the survival probability in the Laplace domain and thus the FPT distribution, which is subsequently checked against the numerical solution of the original problem, and is shown to be in a remarkable agreement with the latter. We note that the symmetries of the geometry under study permit us to express the FPT distribution in a compact form under rather general conditions: for arbitrary radii of the inner and the outer cylinders, for arbitrary starting points, fixed or averaged over the volume or over the cylindrical surface of a given radius, and for an arbitrary chemical reactivity  $\kappa$  defining the probability of a reaction with the target upon encounter.

We illustrate various features of this distribution, *e.g.*, its progressive broadening as the outer cylinder becomes larger, or the size of the target region becomes smaller, and highlight the relevance of the most probable FPT. In addition, our analysis unveils remarkable effects of the chemical reactivity  $\kappa$  on the functional shape of the FPT distribution which were not studied systematically before (Fig. 2). In particular, we proceed to show that upon lowering  $\kappa$ , a plateau-like region develops beyond the most probable FPT, such that, interestingly, the values of the FPT in an interval ranging over several decades turn out to be almost equally probable (see Fig. 5). Moreover, the chosen shape of a capped cylindrical annulus allows us to explore various features of effectively one- (semi-infinite cylindrical annulus), two- (exterior of a capped cylinder), and three-dimensional (exterior of a semi-infinite cylinder) search in unbounded domains, for which the MFPT is infinite. In particular, we recover the characteristic right tails  $t^{-3/2}$  and  $1/(t \ln^2 t)$  of the FPT distribution in effectively one- and two-dimensional geometries.<sup>3</sup> Therefore, our analysis also provides a seminal unifying framework in which the behaviour specific to one-, two- and three-dimensional

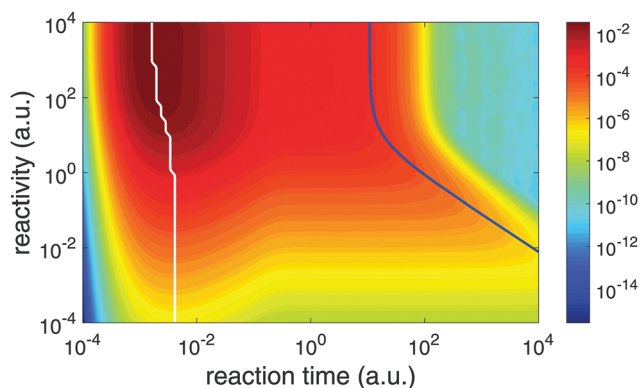


**Fig. 2** Impact of the finite reactivity onto the FPT probability density (shown as a “heatmap”, in which the value of the FPT density is determined by the colour code). When the reactivity decreases, the distribution becomes much broader and extends toward longer reaction times. Blue and white curves show respectively the mean and the most probable FPTs *versus* the reactivity, and differ by orders of magnitude. The FPT probability density was obtained *via* a numerical Laplace inversion of the solution (7).

unbounded systems appears in particular limits. Overall, our results emphasise an absolute necessity of studying the first passage phenomena in biologically relevant systems beyond the MFPT and mean rates, and show that the knowledge of the full FPT distribution is indeed indispensable for getting a complete understanding of the wealth of kinetic behaviour in such systems.

## II. Results

We study the distribution of the FPT to an annular reactive region  $\Gamma$  (the target site) on a cylinder of radius  $\rho$  when diffusion is restricted by an outer, concentric and impermeable cylinder of radius  $R$  (Fig. 1). In other words, diffusion occurs within the confining cylindrical-annulus domain  $\Omega$  spanned by the interval  $z \in (0, L)$  along the cylinder axis and the radius  $r = \sqrt{x^2 + y^2}$  in the interval  $r \in (\rho, R)$ . The target consists of the annular domain  $\Gamma$  on the inner cylinder, specified by the interval  $z \in (0, \varepsilon)$  along the cylinder axis and the radius  $r = \rho$ . Note that the cylindrical domain is capped by reflecting planes at  $z = 0$  and  $z = L$  so that the scenario is in fact equivalent to diffusion in an infinite cylinder with a periodic arrangement of targets. For a particle seeded at some point  $\mathbf{x} \in \Omega$ , the survival probability  $S(\mathbf{x}, t) = \int_{\Omega} P(\mathbf{x}, \mathbf{x}', t) d\mathbf{x}'$  is calculated as the volume integral of the (non-normalised) density function  $P(\mathbf{x}, \mathbf{x}', t)$  to find the particle at position  $\mathbf{x}'$  at time  $t$ . The negative derivative of the survival probability with respect to time then produces the probability density of first passage time,  $H(\mathbf{x}, t) = -\partial S(\mathbf{x}, t)/\partial t$ . In the Laplace domain, defined in terms of  $\tilde{f}(p) = \int_0^{\infty} \exp(-pt)f(t)dt$ , this relation can be rewritten as  $\tilde{H}(\mathbf{x}, p) = 1 - p\tilde{S}(\mathbf{x}, p)$ , where we used the initial condition  $S(\mathbf{x}, t = 0) = 1$ , that is, initially the particle is present in the domain  $\Omega$  with unit probability.

The survival probability, written in cylindrical coordinates  $(r, z, \varphi)$ , satisfies the backward Fokker-Planck equation  $\partial S(\mathbf{x}, t)/\partial t = D\Delta S$ , where  $D$  is the bulk diffusion coefficient, and  $\Delta = \partial_r^2 + r^{-1}\partial_r + \partial_z^2 + r^{-2}\partial_{\varphi}^2$  is the Laplace operator. In the Laplace domain, this equation reduces to the modified Helmholtz equation

$$(p - D\Delta)\tilde{S}(\mathbf{x}, p) = 1. \quad (1)$$

Due to the axial symmetry of the problem, there is no dependence on the polar angle  $\varphi$ . The reflecting boundary conditions at the outer boundaries are taken into account by setting the derivatives  $\partial S/\partial r = 0$  at  $r = R$  and  $\partial S/\partial z = 0$  at  $z = 0, L$ , respectively. To simplify the notations, we replace the axial coordinate  $z$  by  $\theta = \pi z/L$ , and introduce  $\varepsilon = \pi\varepsilon/L$ . The mixed boundary condition on the inner cylinder then reads

$$D(\partial\tilde{S}/\partial r)_{r=\rho} = \begin{cases} \kappa\tilde{S}_{r=\rho} & (0 < \theta < \varepsilon) \\ 0 & (\varepsilon < \theta < \pi) \end{cases} \quad (2)$$

in the Laplace domain. The reactivity coefficient  $\kappa$  under the Robin boundary condition determines the degree of stickiness of the reactive boundary  $\Gamma$  and is associated with the probability of the reaction with the target upon an encounter.<sup>42-44</sup> In standard terms,  $\kappa$  (in units  $\text{m s}^{-1}$ ) is defined as the rate describing the number of

reaction events per unit of time within the volume of the reaction zone around  $\Gamma$ , times the reaction radius and hence, is a material property independent of  $\varepsilon$  (see ref. 45 for more details). For a non-reactive target one has  $\kappa = 0$ , while  $\kappa = \infty$  corresponds to the case of a perfect reaction which, on encounter, occurs with probability 1. We note that the effect of  $\kappa$  on the shape of the full distribution of the FPT is a novel feature here. The only available previous analysis concerned solely its effect on the MFPT, and showed that in related settings it can indeed be decisive.<sup>28,38</sup> This naturally raises the question of the effects of a finite reactivity beyond the MFPT.

We apply an SCA by replacing the mixed boundary condition (2) by the inhomogeneous Neumann condition<sup>37</sup>

$$D(\partial\tilde{S}/\partial r)_{r=\rho} = Q\Theta(\varepsilon - \theta), \quad (3)$$

in which  $\Theta(z)$  is the Heaviside step function and the effective flux  $Q$  remains to be determined by imposing an appropriate self-consistent closure relation,<sup>37</sup> i.e., by requiring that the first line in (2) holds on average:  $D\int_0^{\varepsilon} d\theta(\partial\tilde{S}/\partial r)_{r=\rho} = \kappa\int_0^{\varepsilon} d\theta\tilde{S}_{r=\rho}$ .

We search a solution in the generic form

$$\tilde{S}(r, \theta; p) = \frac{R^2}{D} \left( u_0(r) + \sum_{n=0}^{\infty} a_n g_n(r) \cos n\theta \right), \quad (4)$$

where the first term is the solution of the inhomogeneous problem with Dirichlet boundary conditions at  $r = \rho$ ,  $a_n$  are unknown coefficients to be determined, and  $g_n(r)$  are radial functions satisfying the ordinary differential equation

$$g_n'' + \frac{1}{r}g_n' - \left( \frac{\pi^2 n^2}{L^2} + \frac{s}{R^2} \right) g_n = 0, \quad (5)$$

where the prime denotes the radial derivative and  $s = pR^2/D$  is the dimensionless Laplace variable. We emphasise the dependence of  $u_0(r)$ ,  $a_n$  and  $g_n(r)$  on the Laplace variable, although we do not write it explicitly for the sake of brevity.

The solution of (5) satisfying the boundary condition  $(\partial g_n/\partial r)_{r=R} = 0$  is a linear combination of modified Bessel functions  $I_n(z)$  and  $K_n(z)$  of first and second kind,

$$g_n(r) = I_0(\alpha_n r/L)K_1(\alpha_n R/L) + K_0(\alpha_n r/L)I_1(\alpha_n R/L), \quad (6)$$

with  $\alpha_n = \sqrt{\pi^2 n^2 + sL^2/R^2}$ . The solution of the inhomogeneous problem with Dirichlet boundary conditions at  $r = \rho$  reads  $u_0(r) = [1 - g_0(r)/g_0(\rho)]/s$ .<sup>3,46</sup> The coefficients  $a_n$  are determined and shown in the ESI,<sup>†</sup> Section I, and we obtain the final result for the FPT density

$$\tilde{H}(r, \theta; p) = \eta \frac{g_0(r)}{g_0(\rho)} + 2\eta \frac{g_0'(\rho)}{g_0(\rho)} \sum_{n=1}^{\infty} \frac{g_n(r)}{g_n'(\rho)} \frac{\sin n\varepsilon}{n\varepsilon} \cos(n\theta), \quad (7)$$

in the Laplace domain, where

$$\eta = \left( 1 - \left( \frac{\pi D}{\kappa\varepsilon} + \frac{L}{\pi} \mathcal{R}_\varepsilon \right) \frac{g_0'(\rho)}{g_0(\rho)} \right)^{-1} \quad (8)$$

and

$$\mathcal{R}_\varepsilon = -\frac{2\pi}{L} \sum_{n=1}^{\infty} \frac{g_n(\rho)}{g_n'(\rho)} \left( \frac{\sin n\varepsilon}{n\varepsilon} \right)^2. \quad (9)$$

This approximate representation of the FPT density in the cylindrical-annulus domain is one of the main results of this paper. This result hinges on the SCA, which has already been applied for the analysis of the MFPT in spherical<sup>28</sup> and cylindrical-annulus<sup>38</sup> geometries, and verified against the numerical solution of the mixed boundary problem. Moreover, a similar SCA approach has been used in ref. 45 to calculate the self-propulsion velocity of catalytically active colloids and was shown to be in very good agreement with already known results, only slightly underestimating some insignificant numerical factors. In Section II of the ESI,<sup>†</sup> we show that it is a remarkably accurate approximation for the problem under study, checking it for different initial conditions against the numerical solution of the original mixed boundary value problem.

The moments of this FPT distribution can be obtained from  $\tilde{H}(r, \theta; p)$  in the form  $T_n = (-1)^n \lim_{p \rightarrow 0} (\partial^n / \partial p^n) \tilde{H}(r, \theta; p)$ . The first moment  $T_1$  is the mean FPT that we also denote as  $T$  for brevity. The explicit solution in (7) fully determines the statistics of the FPT. Since  $\tilde{S}(r, \theta; p)$  and the FPT density  $\tilde{H}(r, \theta; p)$  are trivially related in the Laplace domain, we focus on the latter quantity, bearing in mind that all properties of the Laplace-transformed survival probability follow immediately from those of  $\tilde{H}(r, \theta; p)$ . The inverse Laplace transform can be performed either by determining the poles of  $\tilde{H}(r, \theta; p)$  and using the residue theorem, or by numerical inversion using the Talbot algorithm. In Section III of the ESI,<sup>†</sup> we discuss in more detail the former approach, whereas the numerical inversion is used throughout the paper. The solutions in the limiting cases  $R \rightarrow \infty$  and  $L \rightarrow \infty$ , corresponding to effectively two- and one-dimensional geometries, are presented in the ESI<sup>†</sup> (Sections VI and VII).

As already remarked, we will consider different situations with respect to the starting point of the particle. If the starting point is distributed uniformly in the bulk, the volume average of  $\tilde{H}(r, \theta; p)$  can be evaluated exactly,

$$\overline{\tilde{H}(p)} = 2 \int_0^\pi d\theta \int_\rho^R \frac{dr r \tilde{H}(r, \theta; p)}{\pi(R^2 - \rho^2)} = \frac{-2\rho g_0'(\rho)\eta}{s(1 - \rho^2/R^2)g_0(\rho)}, \quad (10)$$

where we used the identity  $\int_\rho^R dr r g_n(r) = -\rho L^2 g_n'(\rho) / \alpha_n^2$ . If in turn the average is taken over uniformly distributed starting points on a cylindrical surface of radius  $r$ , we find

$$\overline{\tilde{H}(p)}_r = \frac{1}{\pi} \int_0^\pi d\theta \tilde{H}(r, \theta; p) = \eta \frac{g_0(r)}{g_0(\rho)}. \quad (11)$$

Setting  $r = \rho$  (when a particle starts from the inner boundary with uniform density), this relation turns out to provide a natural interpretation for the coefficient  $\eta$  defined in (8).

As discussed in ref. 46,  $\tilde{H}(r, \theta; p)$  can also be interpreted as the probability that a mortal walker with bulk killing rate  $p$  reaches the target. For  $p = 0$ , the classical immortal walker reaches the target with unit probability because of the recurrent character

of restricted Brownian motion in a bounded domain. In turn, when  $p > 0$ , the random walker can be killed during its search for the target, and  $\tilde{H}(r, \theta; p)$  is the fraction of walkers that reach the target before being killed.

### III. Discussion

The explicit form of the Laplace-transformed FPT distribution  $\tilde{H}(r, \theta; p)$  in (7) provides unprecedented opportunities for studying the details of the first passage dynamics in a cylindrical-annulus domain. The major challenge here is the relatively large number of relevant parameters of this problem. In fact, the short-time and the long-time behaviours of the FPT distribution (*i.e.*, its left and right tails) strongly depend on the four geometric parameters  $R$ ,  $L$ ,  $\rho$ , and  $\varepsilon$ , as well as on the reactivity  $\kappa$ , and on the starting point (in particular, whether it is fixed or randomly distributed over some subdomain). For instance, the behaviour in the small-target limit  $\varepsilon \rightarrow 0$  is expected to be different from that in the thin cylinder limit  $\rho \rightarrow 0$ . Moreover, one can also investigate the limiting cases of the unbounded exterior of a capped cylinder ( $R \rightarrow \infty$ ), and of an infinitely long cylinder ( $L \rightarrow \infty$ ). In these two limits, the distribution of the FPTs remains well defined, although the MFPT is infinite, as shown in Sections VI and VII of the ESI.<sup>†</sup> We discuss below the various facets of the FPT distribution in different parameter ranges as well as some direct applications.

#### A. General qualitative behaviour

The form of the left tail of the FPT distribution (corresponding to short FPTs) strongly depends on the starting point of the particle. If the starting point is fixed (or surface-averaged with  $r > \rho$ ), the FPTs are dominated by very rare trajectories from  $\mathbf{x}$  to the closest points of the target (called direct trajectories in ref. 32 and 33). As  $t \rightarrow 0$ , we thus expect the behaviour  $H(\mathbf{x}, t) \propto \exp(-|\mathbf{x} - \Gamma|/[4Dt])$ , where  $|\mathbf{x} - \Gamma|$  is the Euclidean distance between the starting point  $\mathbf{x}$  and the target domain  $\Gamma$ . In this limit, the FPT density vanishes very rapidly, meaning that very short FPTs are extremely unlikely. In turn, if the starting point is averaged over the volume or over the inner surface at  $r = \rho$ , such that some particles are initially released right at the surface of the target, one can expect that the FPT density is peaked at  $t = 0$  and then monotonically decreases with  $t$ . In this case, an intermediate power law decay of the FPT distribution is expected. In particular, the general asymptotic behaviour derived in ref. 46 for the perfectly reactive target implies  $\overline{\tilde{H}(p)} \simeq (|\Gamma|/|\Omega|)(p/D)^{-1/2}$ , thus

$$\overline{H(t)} \simeq (2\rho\varepsilon D)\pi^{-3/2}(R^2 - \rho^2)^{-1}(Dt)^{-1/2} \quad (12)$$

as  $t \rightarrow 0$ . In the partially reactive case  $\kappa < \infty$ , the intermediate power-law decay has a different form; see Section III C.

The form of the right tail of the FPT distribution essentially depends on whether the domain  $\Omega$  is bounded or not. For any bounded domain, the spectrum of the governing Laplace operator is discrete, and the FPT density exhibits an exponential decay whose rate is determined by the smallest non-trivial eigenvalue

$\lambda_0$ :  $H(\mathbf{x}, t) \propto \exp(-Dt\lambda_0)$  as  $t \rightarrow \infty$ . In Section III B, we relate the decay rate to the surface-averaged MFPT  $\bar{T}_\rho$ , which is finite. The behaviour is different in the limits  $R \rightarrow \infty$  or  $L \rightarrow \infty$  when the domain  $\Omega$  becomes unbounded. In this case, the MFPT is infinite, and the FPT density exhibits a power-law decay (possibly with logarithmic corrections). We discuss this behaviour in detail in the ESI<sup>†</sup> (see Sections VI and VII). It is important to stress that the related power-law behaviour can also be relevant even for bounded domains as an intermediate regime, before the ultimate exponential cut-off; see also the findings for spherical domains in ref. 32–36. As we will illustrate below, such an intermediate power-law regime can spread over a quite broad range of times and thus be the most interesting feature of the underlying FPT phenomenon. In this situation, the most probable FPT can differ from the MFPT by many orders of magnitude.

### B. The right tail of the FPT distribution

In the limit  $p \rightarrow 0$ , the Laplace transform  $\tilde{H}(r, \theta; p)$  of the FPT density determines both the moments  $T_n$  of the FPT and the long-time behaviour of  $H(r, \theta; t)$  itself. Taking the respective limits of the radial function discussed in Section IV of the ESI<sup>†</sup> we obtain  $\overline{H(t)}_\rho$  as the inverse Laplace transformation of  $\eta$ , namely,

$$\overline{H(t)}_\rho \simeq \exp(-t/\bar{T}_\rho)/\bar{T}_\rho, \quad (13)$$

valid for  $t \rightarrow \infty$ . The characteristic time is given by

$$\bar{T}_\rho = \frac{R^2 - \rho^2}{2D\rho} \left( \frac{\pi D}{\kappa \varepsilon} + \frac{L}{\pi} \mathcal{R}_\varepsilon(p=0) \right), \quad (14)$$

which corresponds to the surface-averaged MFPT investigated in ref. 38. This result is expected for diffusion in a bounded domain. The asymptotic behaviour of other quantities can be obtained in a similar way. For instance,

$$\overline{H(t)}_r \simeq \exp(-t/\bar{T}_r)/\bar{T}_r, \quad (15)$$

with the characteristic time

$$\bar{T}_r = \bar{T}_\rho + \left( \frac{\rho^2 - r^2}{4D} + \frac{R^2 \ln(r/R)}{2D} \right), \quad (16)$$

where the second term in the parentheses is the MFPT to the inner cylinder from a uniformly distributed point at the cylindrical surface at  $r$ . The additivity of two MFPTs reflects the fact that any trajectory from such a point to the target can be split into two independent parts: the path from the cylinder at  $r$  to the cylinder at  $\rho$ , and the path from the cylinder at  $\rho$  to the target, similar to the results for inhomogeneous diffusion in a cylindrical domain.<sup>56</sup>

### C. The left tail of the FPT distribution

The form of the left tail of the FPT distribution stems from the asymptotic behaviour of  $\tilde{H}(r, \theta; p)$  in the limit  $p \rightarrow \infty$ . After the transformations detailed in the ESI<sup>†</sup> (see Section IV), we obtain the Laplace-transformed FPT density  $\tilde{H}(r, \theta; p)$  along with its volume and surface averages,  $\overline{\tilde{H}(p)}$  and  $\overline{\tilde{H}(p)}_r$ . Here one needs to distinguish the cases of perfect ( $\kappa = \infty$ ) and imperfect

( $\kappa < \infty$ ) reactivity at the target. Note that the difference in the asymptotic behaviours for perfectly or only partially reactive targets was discussed for other geometries in ref. 57 and 58.

**1. Perfect reactions.** According to (11) the inverse Laplace transform of asymptotic relation (S34) in the ESI<sup>†</sup> yields the asymptotic behaviour of the surface-averaged FPT density  $\overline{H(t)}_\rho$  at small  $t$ , namely,

$$\overline{H(t)}_\rho \simeq (\varepsilon/\pi)\delta(t) + (D/[8\pi])^{1/2} L^{-1} t^{-1/2} + O(1). \quad (17)$$

The first term represents the fraction  $\varepsilon/\pi$  of particles that started right at the target, for which the first passage time is zero. The next term accounts for the FPTs of particles with non-zero initial separations from the target. Since (S33), ESI<sup>†</sup> was derived for  $\varepsilon \leq \pi/2$ , the above asymptotic behaviour is not applicable for the case  $\varepsilon = \pi$ , for which  $\overline{H(t)}_\rho = \delta(t)$  without correction terms.

When the particles start from a cylindrical surface at  $r$ , (11) has an extra factor  $g_0(r)/g_0(\rho)$ . With the large- $p$  asymptotic (S36), ESI<sup>†</sup> we find the short-time behaviour

$$\begin{aligned} \overline{H(t)}_r &\simeq \frac{\varepsilon}{\pi} (\rho/[4\pi r D t^3])^{1/2} \exp(-(r-\rho)^2/[4Dt]) \\ &\times \left( r - \rho + Dt \left( \frac{\pi}{\sqrt{2}L\varepsilon} + \frac{\sqrt{1/\rho} - \sqrt{1/r}}{4\sqrt{R}} \right) + O(t^2) \right). \end{aligned} \quad (18)$$

Fig. 3(a) shows the surface-averaged probability density  $\overline{H(t)}_r$  for two choices of the target height:  $\varepsilon = 0.2$  and  $\varepsilon = \pi$ . The latter case describes the whole inner cylinder as reactive, while the former value of  $\varepsilon$  is chosen arbitrarily and meant to illustrate a moderately small target. In both cases shown in the figure, the short-time asymptotic (18) is very accurate up to  $Dt/R^2 \lesssim 0.1$ . When the target is the entire inner cylinder ( $\varepsilon = \pi$ ), this time scale is of the order of the corresponding MFPT  $D\bar{T}_r/R^2 \approx 0.34$ . For times of that order the FPT density has an exponential cut-off. For the case of a partially reactive inner cylinder ( $\varepsilon = 0.2$ ), the MFPT is, notably, around four decades longer than the most likely FPT.

For the volume average, (10), together with (S34) (ESI<sup>†</sup>), yields a different short-time behaviour, namely,

$$\overline{H(t)} \simeq \frac{\rho D}{R^2 - \rho^2} \left( \frac{2\varepsilon}{\pi\sqrt{\pi D t}} + \left( \frac{1}{\sqrt{2}L} + \frac{\varepsilon}{\pi\rho} \right) + O(t^{1/2}) \right). \quad (19)$$

The leading term agrees with the general behaviour in (12). Fig. 3(b) shows the FPT density obtained by numerical inversion of  $\tilde{H}(p)$  from (7). In the particular case  $\varepsilon = \pi$  (the entire inner cylinder is absorbing), one has  $a_n = 0$  and thus (7) is exact. One can see that both distributions are broad. The asymptotic (19) is remarkably accurate for both cases  $\varepsilon = \pi$  and  $\varepsilon = 0.2$ .

**2. Imperfect reactions.** For imperfect reactions with finite reactivity  $\kappa$ , the first arrival onto the target does not necessarily imply a successful reaction, so that the reaction times are increased. Indeed, for  $\kappa < \infty$ , (S33) in the ESI<sup>†</sup> acquires the

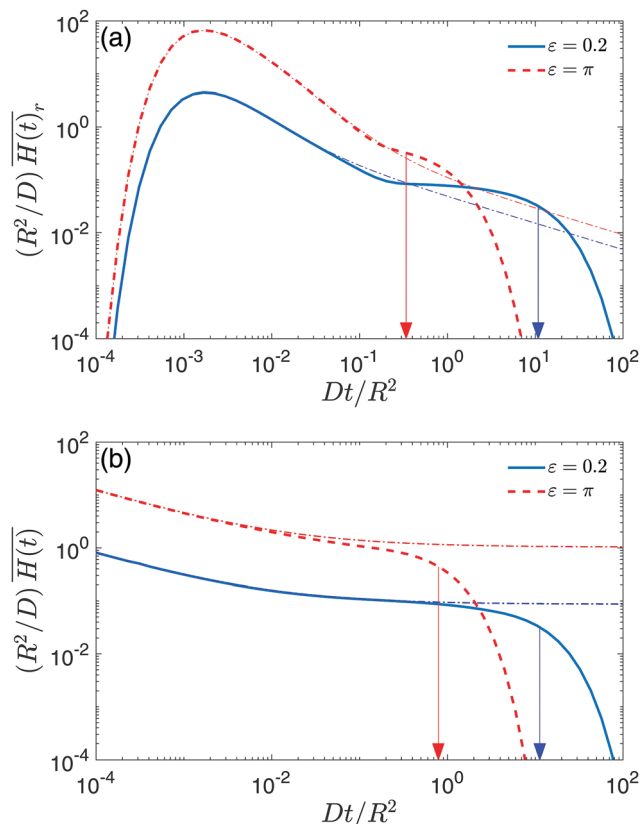


Fig. 3 Surface-averaged (a) and volume-averaged (b) FPT densities  $\overline{H(t)}_r$  and  $\overline{H(t)}$  as functions of  $t$  for perfect reactions ( $\kappa = \infty$ ) with  $L/R = \pi$ ,  $\rho/R = 0.1$ ,  $r/R = 0.2$ , and  $\varepsilon = 0.2$  (solid line) and  $\varepsilon = \pi$  (dashed line). Both curves are obtained by the numerical Laplace inversion of (7). The two arrows indicate the MFPT  $D\overline{T}_r/R^2$  for both cases: 10.82 ( $\varepsilon = 0.2$ ) and 0.34 ( $\varepsilon = \pi$ ) for the surface-averaged quantity, and 11.27 ( $\varepsilon = 0.2$ ) and 0.79 ( $\varepsilon = \pi$ ) for the volume-averaged quantity. The dash-dotted lines indicate the short-time asymptotic (18) and (19), and agree very well with the general result in (7) well beyond the most probable FPT. Length and time scales are fixed by setting  $R = 1$  and  $R^2/D = 1$ .

asymptotic (S37),  $\text{ESI}^\dagger$  from which we get the short-time behaviours

$$\overline{H(t)}_\rho \simeq \frac{\varepsilon}{\pi} \frac{\kappa}{\sqrt{\pi D t}} - \frac{\varepsilon}{\pi} \left( \frac{\kappa^2}{D} + \frac{\kappa}{2\rho} \right) + O(\sqrt{t}), \quad (20a)$$

$$\overline{H(t)}_r \simeq \frac{\varepsilon}{\pi} \sqrt{\rho/r} \frac{\kappa}{\sqrt{\pi D t}} \exp\left(-\frac{(r-\rho)^2}{4Dt}\right), \quad (20b)$$

$$\overline{H(t)} \simeq \frac{2\rho\varepsilon\kappa}{\pi(R^2 - \rho^2)} \left( 1 - \frac{2\kappa\sqrt{Dt}}{D\sqrt{\pi}} + O(t) \right). \quad (20c)$$

Interestingly, for imperfect reactions the leading short-time behaviour of the FPT distribution appears to be distinctly different, depending on the starting point:  $\overline{H(t)}_\rho$  diverges as  $t \rightarrow 0$ ,  $\overline{H(t)}_r$  tends to zero in this limit, while  $\overline{H(t)}$  approaches a constant value.

Fig. 4(a) shows the surface-averaged FPT density  $\overline{H(t)}_r$  at  $r/R = 0.2$  and  $\kappa R/D = 1$ . One can see that the short-time asymptotic (20b) accurately reproduces the behaviour of this

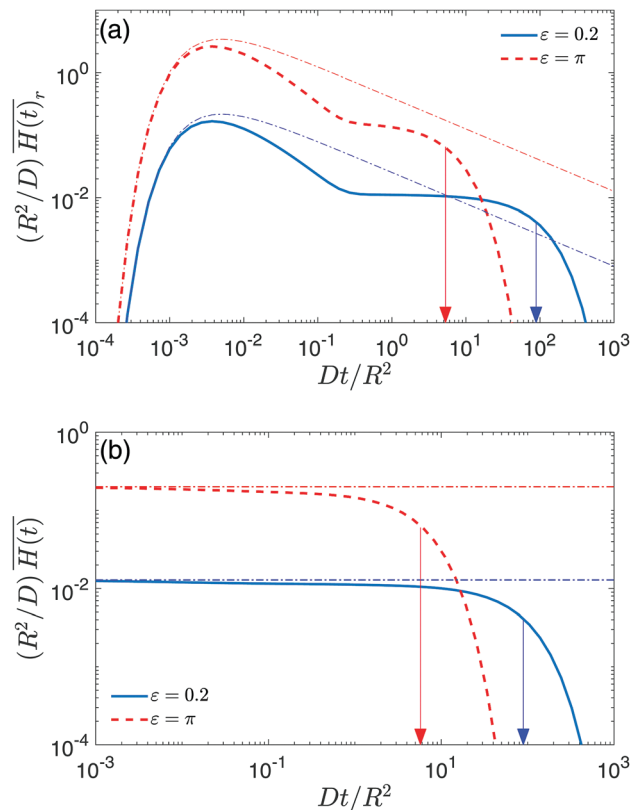


Fig. 4 Surface-averaged (a) and volume-averaged (b) FPT densities  $\overline{H(t)}_r$  and  $\overline{H(t)}$  as functions of  $t$  for imperfect reactions ( $\kappa R/D = 1$ , cf. Fig. 3), with  $L/R = \pi$ ,  $\rho/R = 0.1$ ,  $r/R = 0.2$ , and  $\varepsilon = 0.2$  (solid line) and  $\varepsilon = \pi$  (dashed line). Both curves are obtained by numerical Laplace inversion of (7). The two arrows indicate the MFPT  $D\overline{T}_r/R^2$  for both cases: 88.58 ( $\varepsilon = 0.2$ ) and 5.29 ( $\varepsilon = \pi$ ) for surface-averaged quantity, and 89.03 ( $\varepsilon = 0.2$ ) and 5.74 ( $\varepsilon = \pi$ ) for volume-averaged quantity. The dash-dotted lines show the short-time asymptotic (20b) and (20c) (in which only the leading term is kept). The length and time scales are fixed by setting  $R = 1$  and  $R^2/D = 1$ .

density up to its maximum. As a consequence, the position  $t_m$  of this maximum can be obtained by taking the derivative of (20b) with respect to  $t$  and setting the resulting expression equal to zero. This gives the following estimate for the most probable FPT:

$$t_m = (r - \rho)^2 / (2D). \quad (21)$$

The estimated value of  $t_m$  in (21) depends only on the distance to the target but does not depend on either the target size  $\varepsilon$  or the reactivity  $\kappa$ , nor on the inner radius of the cylinder. In this example,  $Dt_m/R^2 = 0.005$ , whereas the MFPT is four orders of magnitude higher. Similar to the findings in ref. 32, the most likely FPT corresponds to geometry-controlled direct trajectories, in which the initial distance from the target is decisive.

We also note that the probability density is broader in the case  $\varepsilon = 0.2$ , with a flat intermediate region between the maximum hump and the exponential cut-off (in the region  $0.2 \leq Dt/R^2 \leq 10$ ). As the target size  $\varepsilon$  or the reactivity  $\kappa$  decreases, the MFPT increases and thus the exponential cut-off moves towards longer times. In turn, the position and shape of the maximum remain approximately constant (dominated by the initial distance and the diffusivity  $D$ ) so

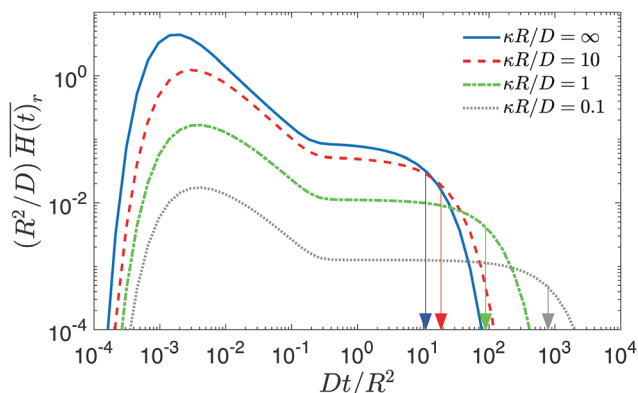


Fig. 5 Surface-averaged FPT density  $\overline{H(t)}_r$  as a function of  $t$  for imperfect reactions, with  $L/R = \pi$ ,  $\rho/R = 0.1$ ,  $r/R = 0.2$ , and  $\varepsilon = 0.2$ . All curves are obtained by numerical Laplace inversion of (7). Arrows indicate the MFPT  $D\overline{T}_r/R^2$ : 10.82 ( $\kappa = \infty$ ), 18.60 ( $\kappa = 10$ ), 88.58 ( $\kappa R/D = 1$ ), and 788.36 ( $\kappa R/D = 0.1$ ). Note that (at fixed  $D$ ) the MFPT grows with decreasing  $\kappa$ . In this regime, the MFPT becomes dominated by chemical reactivity,  $\overline{T}_r \sim 1/\kappa$  (see ref. 28 and 38). The most probable FPT exhibits a weak dependence on  $\kappa$ . Note also the appearance of a pronounced plateau-like region, which stretches over progressively longer time scales upon lowering the reactivity  $\kappa$ . Hence, there is a broad range of times with equiprobable realisations of the FPT. The length and time scales are fixed by setting  $R = 1$  and  $R^2/D = 1$ .

that the intermediate region expands, as we checked for  $\varepsilon = 0.05$  and for  $\kappa R/D = 0.1$  (not shown). This is a striking result: if the particle does not manage to find the target and react within short times comparable to  $t_m$  (around the maximum), it explores the entire confining domain with eventual returns to the target. As a consequence, its reaction time is distributed almost uniformly over a very broad range of times, up to the exponential cut-off which is essentially determined by the MFPT. The latter, in turn, is dominated by the chemical reactivity, while the diffusive search for the target provides only a sub-dominant contribution<sup>38</sup> (see also ref. 28 for a general discussion). One can see that the low reactivity  $\kappa$  leads to a homogenisation of the search process, as evidenced in Fig. 5, and the plateau-like region past the most probable FPT extends over progressively longer scales when  $\kappa$  becomes smaller. As a consequence, the values of FPTs ranging over several orders of magnitude appear to be almost equally probable.

Fig. 4(b) shows that the volume-averaged FPT density  $\overline{H(t)}$  remains almost constant at short times and then has an exponential cut-off. This almost uniform behaviour at short times resembles that shown in Fig. 4(a). The only difference is that there is no maximum at short times as some particles start infinitely close to the target.

#### D. Biological implications

The function of biological cells to a large extent relies on the passive diffusion of regulatory molecules. In particular, the expression level of any gene is controlled by the binding of transcription factor proteins. Inside the chromosome a transcription factor locates its specific binding site *via* facilitated diffusion combining volume search with one-dimensional sliding along the DNA, as well as

intersegmental jumps.<sup>47–49</sup> As many bacteria cells such as the well-studied *E. coli* or *bacilli* have distinct cylindrical shapes, the analysis here provides an answer to the question how fast a given transcription factor can reach the chromosome from the cytoplasm of the cell in the first place. Our results demonstrate that for all considered scenarios the FPT to the nucleoid is broadly distributed and may deviate significantly from the respective MFPT. For reliable regulation it may thus be advantageous that transcription factors, which often occur in very low copy numbers in a cell, are inhomogeneously distributed in the cell,<sup>50,51</sup> and may thus be kept close to their target site on the DNA. This reasoning is in accord with the results for the downstream gene regulation model in ref. 52, supporting the rapid search hypothesis<sup>53</sup> as well as the geometry controlled few-encounter scenario of ref. 32.

We also mention another relevant system for the cylindrical geometry, namely, axons, the up to a meter long protrusion of neuronal cells, whose diameter may span from 0.1  $\mu\text{m}$  up to 20  $\mu\text{m}$ .<sup>54</sup> In the giant squid, the diameter may even reach the macroscopic size of 1 mm. In such an axon, motor proteins detach from the central bundle of microtubules, along which the motors actively transport cargoes. The motors' reattachment dynamics after unbinding, governed by the results derived herein for imperfect reactions, have been shown to be important for the observed Lévy walk transport.<sup>55</sup>

## IV. Conclusion

Although the necessity of knowing the full FPT distribution, especially in situations when several length scales are involved, has been emphasised earlier (*e.g.*, in ref. 7, 8, 32, and 33), not much progress has been achieved in this direction. For the first time, we discuss here, using an analytical solution, the forms of the full first-passage time distribution for different initial conditions in a cylindrical-annulus geometry relevant for bacteria cells and neuronal axons. Due to the quite large number of parameters in the system, the full distribution of the FPT has a complicated structure and appreciably changes its shape when the parameters are changed. It would therefore be naive to expect that the full complexity of the behaviour in the system could be exhaustively characterised by just the first moment of this distribution – the mean first-passage time – on which the previous research has concentrated almost exclusively.

Within a self-consistent approach, proposed originally in a completely different context in ref. 37, we found explicit, approximate expressions for the full FPT distribution, which we validated by extensive numerical analysis. One of the main features that we uncovered is that, indeed, the full distribution has an important structure and is rather sensitive to a slight variation of the system's parameters. Next, we showed that the MFPT turns out to be several orders of magnitude longer than the most likely FPT, the decisive quantity indicating when typically the first molecule arrives at the target and triggers biochemical follow-up reactions. Therefore, while the knowledge of the MFPT is certainly helpful and important, it carries the

danger of being misleading, given that the MFPT largely overestimates the typical time scales involved in cellular processes. In this context, former theoretical works devoted to the minimisation of the MFPT do not necessarily reveal the optimal conditions for the function of biological systems, because they do not affect the most likely FPT.

An equally significant result of our analysis is the occurrence of an extended plateau of the FPT distribution for lower reactivity constants  $\kappa$ , signifying that over more than a decade all FPTs within this range become equally probable and thus the triggering events even more unfocused. Moreover, within the unique geometric setting, we could unveil intriguing dimensionality features of the diffusive search in unbounded domains, for which the MFPT is infinite and thus useless. The derived asymptotic formulas correctly describe intermediate regimes of the FPT distribution in the bounded case as well.

Having available expressions for the full FPT distribution will allow a more faithful evaluation of measured reaction dynamics, but also the planning of new experiments, in particular, when single molecule resolution is accessible. We expect that our results will lead to a new level of quantitative understanding of molecular regulation processes on microscopic levels, for instance, a renormalisation of rate constants extracted from MFPT interpretations.

## Conflicts of interest

There are no conflicts to declare.

## Acknowledgements

DSG acknowledges the support under Grant No. ANR-13-JSV5-0006-01 of the French National Research Agency. RM acknowledges support from the Deutsche Forschungsgemeinschaft through projects ME 1535/6-1 and ME 1535/7-1, as well as from the Foundation for Polish Science within an Alexander von Humboldt Polish Honorary Research Fellowship.

## References

- 1 B. Alberts, A. Johnson, J. Lewis, D. Morgan, M. Raff, K. Roberts and P. Walter, *Molecular Biology of the Cell*, Garland Science, New York, NY, 2014.
- 2 D. P. Snustad and M. J. Simmons, *Principles of Genetics*, Wiley, New York, 2000.
- 3 S. Redner, *A Guide to First Passage Processes*, Cambridge University Press, Cambridge, 2001.
- 4 R. Metzler, G. Oshanin and S. Redner, *First-Passage Phenomena and Their Applications*, World Scientific, Singapore, 2014.
- 5 D. Holcman and Z. Schuss, Control of flux by narrow passages and hidden targets in cellular biology, *Rep. Prog. Phys.*, 2013, **76**, 074601.
- 6 P. C. Bressloff and J. M. Newby, Stochastic models of intracellular transport, *Rev. Mod. Phys.*, 2013, **85**, 135–196.
- 7 O. Bénichou, C. Loverdo, M. Moreau and R. Voituriez, Intermittent search strategies, *Rev. Mod. Phys.*, 2011, **83**, 81.
- 8 O. Bénichou and R. Voituriez, From first-passage times of random walks in confinement to geometry-controlled kinetics, *Phys. Rep.*, 2014, **539**, 225–284.
- 9 J. Yu, J. Xiao, X. Ren, K. Lao and X. S. Xie, Probing Gene Expression in Live Cells, One Protein Molecule at a Time, *Science*, 2006, **311**, 1600.
- 10 G.-W. Li and X. S. Xie, Central dogma at the single-molecule level in living cells, *Nature*, 2011, **475**, 308.
- 11 A. Raj and A. van Oudenaarden, Nature, Nurture, or Chance: Stochastic Gene Expression and Its Consequences, *Cell*, 2008, **135**, 216.
- 12 M. J. Ward and J. B. Keller, Strong Localized Perturbations of Eigenvalue Problems, *SIAM J. Appl. Math.*, 1993, **53**, 770–798.
- 13 I. V. Grigoriev, Y. A. Makhnovskii, A. M. Bereshkovskii and V. Y. Zitserman, Kinetics of escape through a small hole, *J. Chem. Phys.*, 2002, **116**, 9574.
- 14 A. Singer, Z. Schuss, D. Holcman and R. S. Eisenberg, Narrow Escape, Part I, *J. Stat. Phys.*, 2006, **122**, 437–463.
- 15 A. Singer, Z. Schuss and D. Holcman, Narrow Escape, Part II The circular disk, *J. Stat. Phys.*, 2006, **122**, 465–489.
- 16 A. Singer, Z. Schuss and D. Holcman, Narrow Escape, Part III Riemann surfaces and non-smooth domains, *J. Stat. Phys.*, 2006, **122**, 491–509.
- 17 S. Condamin, O. Bénichou, V. Tejedor, R. Voituriez and J. Klafter, First-passage time in complex scale-invariant media, *Nature*, 2007, **450**, 77.
- 18 O. Bénichou and R. Voituriez, Narrow-Escape Time Problem: Time Needed for a Particle to Exit a Confining Domain through a Small Window, *Phys. Rev. Lett.*, 2008, **100**, 168105.
- 19 S. Pillay, M. J. Ward, A. Peirce and T. Kolokolnikov, An Asymptotic Analysis of the Mean First Passage Time for Narrow Escape Problems: Part I: Two-Dimensional Domains, *SIAM Multi. Model. Simul.*, 2010, **8**, 803–835.
- 20 A. F. Cheviakov, M. J. Ward and R. Straube, An Asymptotic Analysis of the Mean First Passage Time for Narrow Escape Problems: Part II: The Sphere, *SIAM Multi. Model. Simul.*, 2010, **8**, 836–870.
- 21 G. Oshanin, M. Tamm and O. Vasilyev, Narrow-escape times for diffusion in microdomains with a particle-surface affinity: Mean-field results, *J. Chem. Phys.*, 2010, **132**, 235101.
- 22 A. F. Cheviakov, A. S. Reimer and M. J. Ward, Mathematical modeling and numerical computation of narrow escape problems, *Phys. Rev. E: Stat., Nonlinear, Soft Matter Phys.*, 2012, **85**, 021131.
- 23 C. Caginalp and X. Chen, Analytical and Numerical Results for an Escape Problem, *Arch. Ration. Mech. Anal.*, 2012, **203**, 329–342.
- 24 A. M. Berezhkovskii and L. Dagdug, Effect of binding on escape from cavity through narrow tunnel, *J. Chem. Phys.*, 2012, **136**, 124110.
- 25 A. M. Berezhkovskii and A. V. Barzykin, Search for a small hole in a cavity wall by intermittent bulk and surface diffusion, *J. Chem. Phys.*, 2012, **136**, 054115.

- 26 D. S. Grebenkov, Universal formula for the mean first passage time in planar domains, *Phys. Rev. Lett.*, 2016, **117**, 260201.
- 27 T. Guérin, N. Levernier, O. Bénichou and R. Voituriez, Mean first-passage times of non-Markovian random walkers in confinement, *Nature*, 2016, **534**, 356–359.
- 28 D. S. Grebenkov and G. Oshanin, Diffusive escape through a narrow opening: new insights into a classic problem, *Phys. Chem. Chem. Phys.*, 2017, **19**, 2723–2739.
- 29 T. Agranov and B. Meerson, Narrow escape of interacting diffusing particles, *Phys. Rev. Lett.*, 2018, **120**, 120601.
- 30 D. Holcman and Z. Schuss, The Narrow Escape Problem, *SIAM Rev.*, 2014, **56**, 213–257.
- 31 Z. Schuss, A. Singer and D. Holcman, The narrow escape problem for diffusion in cellular microdomains, *Proc. Natl. Acad. Sci. U. S. A.*, 2007, **104**, 16098–16103.
- 32 A. Godec and R. Metzler, Universal Proximity Effect in Target Search Kinetics in the Few-Encounter Limit, *Phys. Rev. X*, 2016, **6**, 041037.
- 33 A. Godec and R. Metzler, First passage time distribution in heterogeneity controlled kinetics: going beyond the mean first passage time, *Sci. Rep.*, 2016, **6**, 20349.
- 34 C. Mejía-Monasterio, G. Oshanin and G. Schehr, First passages for a search by a swarm of independent random searchers, *J. Stat. Mech.*, 2011, P06022.
- 35 T. Mattos, C. Mejía-Monasterio, R. Metzler and G. Oshanin, First passages in bounded domains: When is the mean first passage time meaningful?, *Phys. Rev. E: Stat., Nonlinear, Soft Matter Phys.*, 2012, **86**, 031143.
- 36 T. Mattos, C. Mejía-Monasterio, R. Metzler, G. Oshanin and G. Schehr, Trajectory-to-trajectory fluctuations in first-passage phenomena in bounded domains, in ref. 4.
- 37 D. Shoup, G. Lipari and A. Szabo, *Biophys. J.*, 1981, **36**, 697.
- 38 D. S. Grebenkov, R. Metzler and G. Oshanin, Effects of the target aspect ratio and intrinsic reactivity onto diffusive search in bounded domains, *New J. Phys.*, 2017, **19**, 103025.
- 39 J.-F. Rupprecht, O. Bénichou, D. S. Grebenkov and R. Voituriez, Exit time distribution in spherically symmetric two-dimensional domains, *J. Stat. Phys.*, 2015, **158**, 192–230.
- 40 S. A. Isaacson and J. Newby, Uniform asymptotic approximation of diffusion to a small target, *Phys. Rev. E: Stat., Nonlinear, Soft Matter Phys.*, 2013, **88**, 012820.
- 41 A. E. Hafner and H. Rieger, Spatial cytoskeleton organization supports targeted intracellular transport, *Biophys. J.*, 2018, **114**, 1420–1432.
- 42 D. S. Grebenkov, M. Filoche and B. Sapoval, Spectral Properties of the Brownian Self-Transport Operator, *Eur. Phys. J. B*, 2003, **36**(2), 221–231.
- 43 D. S. Grebenkov, Partially Reflected Brownian Motion: A Stochastic Approach to Transport Phenomena, in *Focus on Probability Theory*, ed. L. R. Velle, Nova Science Publishers, 2006, pp. 135–169.
- 44 D. S. Grebenkov, Residence times and other functionals of reflected Brownian motion, *Phys. Rev. E: Stat., Nonlinear, Soft Matter Phys.*, 2007, **76**, 041139.
- 45 G. Oshanin, M. N. Popescu and S. Dietrich, Active colloids in the context of chemical kinetics, *J. Phys. A: Math. Theor.*, 2017, **50**, 134001.
- 46 D. S. Grebenkov and J.-F. Rupprecht, The escape problem for mortal walkers, *J. Chem. Phys.*, 2017, **146**, 084106.
- 47 P. H. von Hippel and O. G. Berg, Facilitated target location in biological systems, *J. Biol. Chem.*, 1989, **264**, 675–678.
- 48 J. Elf, G. W. Li and X. S. Xie, Probing transcription factor dynamics at the single-molecule level in a living cell, *Science*, 2007, **316**, 1191–1194.
- 49 M. A. Lomholt, B. v. d. Broek, S.-M. J. Kalisch, G. J. L. Wuite and R. Metzler, Facilitated diffusion with DNA coiling, *Proc. Natl. Acad. Sci. U. S. A.*, 2009, **106**, 8204.
- 50 F. Képès, Periodic transcriptional organization of the *E. coli* genome, *J. Mol. Biol.*, 2004, **340**, 957–964.
- 51 T. E. Kuhlman and E. C. Cox, Gene location and DNA density determine transcription factor distributions in *Escherichia coli*, *Mol. Syst. Biol.*, 2012, **8**, 610.
- 52 O. Pulkkinen and R. Metzler, Distance matters: the impact of gene proximity in bacterial gene regulation, *Phys. Rev. Lett.*, 2013, **110**, 198101.
- 53 G. Kolesov, Z. Wunderlich, O. N. Laikova, M. S. Gelfand and L. A. Mirny, How gene order is influenced by the biophysics of transcription regulation, *Proc. Natl. Acad. Sci. U. S. A.*, 2007, **104**, 13948.
- 54 L. Squire, *Fundamental neuroscience*, Academic Press, Amsterdam, 2013.
- 55 K. Chen, B. Wang and S. Granick, Memoryless self-reinforcing directionality in endosomal active transport within living cells, *Nat. Mater.*, 2015, **14**, 589–593.
- 56 A. Godec and R. Metzler, Optimization and universality of Brownian search in a basic model of quenched heterogeneous media, *Phys. Rev. E: Stat., Nonlinear, Soft Matter Phys.*, 2015, **91**, 052134.
- 57 D. S. Grebenkov, Subdiffusion in a bounded domain with a partially absorbing-reflecting boundary, *Phys. Rev. E: Stat., Nonlinear, Soft Matter Phys.*, 2010, **81**, 021128.
- 58 D. S. Grebenkov, Searching for partially reactive sites: Analytical results for spherical targets, *J. Chem. Phys.*, 2010, **132**, 034104.